

Unsupervised Multiphase Segmentation: a phase balancing model

1

Berta Sandberg Sung Ha Kang Tony F. Chan

Abstract

Variational Models have been studied for image segmentation since the Mumford-Shah functional was introduced in the late 1980's. In this paper, we focus on multiphase segmentation with a new regularization term that yields a unsupervised segmentation model. We propose a functional that simultaneously chooses a reasonable number of phases while segmenting the image. By using the scale measure of the phases in the regularization term, bigger objects are preferred to be identified while segmentation is driven by the intensity fitting term. For the numerical method, we propose a fast brute-force algorithm, and we present experiments showing the robustness of this method.

I. INTRODUCTION

Image segmentation separates the image into different regions to simplify the image and identify the objects easily. Image segmentation has been extensively studied via various approaches, such as mixture random-field models [10], Mumford and Shah's variational image model [17], and new segmentation models incorporates more complexities, like Monte-Carlo Markov chain model [27], the graph-cutting and spectral method [23], and the variational texture segmentation models [20], [21], just to mention a few. Many extensions and properties have been studied for the variational approaches since the work of Mumford and Shah's image segmentation model. The Chan-Vese model [6] is well-known for a successful level set implementation, and this work has been extended to various cases such as multi-channel [5], texture segmentation [20], a logic model [19] and multiphase segmentations [7], [28].

Sandberg is with Adel Research and Department of Mathematics, University of California, Los Angeles (berta.sandberg@adelresearch.com), Kang (the corresponding author) is with the School of Mathematics, Georgia Institute of Technology, Atlanta, GA 30332 (kang@math.gatech.edu) and Chan is with the Department of Mathematics, University of California, Los Angeles, Los Angeles, CA 90024, (chan@math.ucla.edu). This work has been partially supported by NSF:DMS-0908517, ONR:N00014-06-1-0345, and NSF:DMS-0610079.

In this paper, we focus on multiphase image segmentation, that is to identify more than two phases from a given image. There are several region-based multiphase segmentation models introduced by various researchers, such as Vese and Chan [28], Chung and Vese [7], Brox and Weickert [2], Tai and Chan [26], Lie, Lysaker and Tai [16], Jung, Kang and Shen [13], and Bae and Tai [1]. In [28], Vese and Chan first introduced the generalization of two-phase segmentation model [6] by using $\log_2 n$ number of level sets to identify n number of phases. A multi-layer method is introduced in [7], where the authors used more than one levels of a level set to represent the discontinuity of the image, inspired by modeling island dynamics for epitaxial growth. In [2], the authors proposed a minimization strategy using the level set framework for minimizing the energy of [29]. In [16], a piecewise level set method is introduced which uses one level set for multiphase segmentation by representing each phase with a different constant value. The graph-cut algorithm is utilized for multiphase Mumford-Shah model in [1]. In [13], the authors introduced a relaxed model for multiphase segmentation using Γ -convergence analysis. More related work can be found at [3], [9], [14], [15], [18].

Let Ω be the image domain, a bounded Lipschitz domain, and $u_o : \Omega \rightarrow \mathbb{R}_+ \cup \{0\}$ be a given image. Recall that the classical Mumford-Shah segmentation is to minimize

$$\mathcal{E}_{ms}[u, \Gamma | u_o] = \alpha \int_{\Omega \setminus \Gamma} |\nabla u|^2 dx + \beta \mathcal{H}^1(\Gamma) + \int_{\Omega} (u - u_o)^2 dx, \quad (1)$$

where $\Gamma \in \Omega$ denotes the *edge set* of the image u , and \mathcal{H}^1 represents the 1-dimensional Hausdorff measure. Multiphase segmentation identifies different phases by the intensity discontinuities, and this setting is considered in [7], [13], [16], [26], [28]. For identifying piecewise constant objects, the reduced Mumford-Shah functional can be written as, minimizing

$$\mathcal{E}_{cv}[u, \Gamma | u_o] = \beta \mathcal{H}^1(\Gamma) + \sum_{i=1}^N \int_{\Omega_i} |u_o - c_i|^2, \quad (2)$$

where Ω_i s are the connected components of $\Omega \setminus \Gamma$ and c_i is the intensity average of u in each Ω_i . With a successful level-set implementation, this reduced Mumford-Shah model is also frequently referred to as the Chan-Vese (CV) model for a two-phase case [6]. This particular expression of multiphase segmentation (2) is first used in [16] and shown it can keep symmetry for triple junctions.

One of the limitation of these multiphase segmentation methods is that the number of phases are typically given or needs to be chosen a priori, to get a proper result. One way to avoid choosing the number of phases is to give many initial contours with the hope that only the necessary contours will remain. In practice, if more phases are given than needed, then over-segmentation occurs, as illustrated

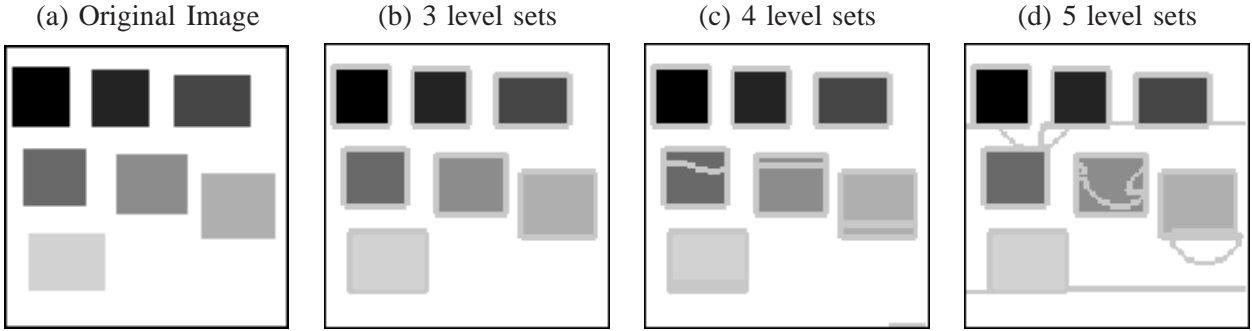


Fig. 1. (a) The original given image is a piecewise constant image with eight different constant intensities. (b), (c) and (d) shows three different possible segmentation results using [28] with different numbers of level sets: (b) 3 level sets, (c) 4 level sets, and (d) 5 level sets. Boundaries of contours are superposed over the segmented result. (b) shows segmentation using 3 level sets ($2^3 = 8$ phases), exactly finding the correct segmentation. When more contours are used than needed, as in (c) and (d), one object can be separated to more than one segments and there are many empty level sets.

in Figure I. The algorithm unnecessarily separates one object to more than one regions. Figure I is using multiphase level set segmentation as in [28]. In [13], [16], typically a reasonable number of phases are given before the experiments or some supervisions are used for good segmentation results. Another possibility of avoiding over-segmentation is to gradually increase the number of phases one by one. Then, in most cases, the intensity fitting term will drive the segmentation and even slight different in intensity can continuously increase the number of phases. In addition, for the functional models, such as (1) and (2), there are at least one free parameter to choose and, often for multiphase segmentation, the result becomes very sensitive to the choice of these parameters. In [2], the authors also noticed the difficulties of having arbitrary number of regions, and proposed a minimization strategy using level set method for minimizing the energy of [29].

We propose a new model for unsupervised segmentation, which automatically chooses the number of phases without any user input. This model gives reasonable number of phases while segmenting the image at the same time. The contribution of this paper is to propose a new variational functional for unsupervised multiphase segmentation and provide a fast numerical algorithm. We present a brute-force algorithm for a fast and easy computation without using Euler-Lagrange equation of this nonlinear functional. The numerical experiments are presented to validate the proposed functional.

This paper is organized as follows. In Section II, followed by a general formulation of multiphase segmentation, we present a new phase balancing unsupervised multiphase segmentation model in subsec-

tion II-C. In Section III, we present the details of the brute-force algorithm. This is followed by various numerical experiments in Section IV.

II. UNSUPERVISED MULTIPHASE SEGMENTATION MODEL

We represent the segmented image as a linear combination of different phases which are defined by characteristic functions as χ_i to be representing each phase. The $\sum \chi_i$ covers the entire image domain Ω and $\chi_i \cap \chi_j = \emptyset$. Each χ_i is defined by one intensity average value c_i , and each phase may consist of many separate regions (distinct connected components). The average value is computed by $c_i = \int_{\chi_i} u_o(x)dx / \int_{\chi_i} 1dx$ as usual. Then, the final segmented result is represented as

$$u = \sum_{i=1}^K c_i * \chi_i.$$

In the CV model (2), the main two terms represent the intensity fitting term and the regularization term. The segmentation is driven by the intensity, while the length of the boundaries are kept to be minimized to avoid oscillatory boundary identification. We also keep these two terms for our segmentation model and construct our new functional based on this CV model (2). We propose to add two more objectives to design an unsupervised model, which automatically gives the number of phases as well as the segmentation of the image. The objectives are as follows:

- 1) [Phase] Find the objects with significant sizes. We prefer not to have small partitions of the image, but want to identify relatively big objects which can be understood as a feature of the image.
- 2) [Balance] We assume each identified phases are all equally important, i.e. no a priory information is given on which phase is more important than the other. Therefore, this functional should partition the image uniformly among different phases.

In the following subsections, we construct the new functional by implementing the above two new objectives.

A. Phase

We turn our attention to the scale term which has been studied in [25] to identify objects of big enough size. The authors of [25] have recognized the relation between the length and the area of objects, and the scale term is defined as $scale := \frac{area}{length}$. When the size of an object is big, the scale value is big, and when an object is small, the scale value is small. This term is analyzed in the context of total variation (TV) denoising.

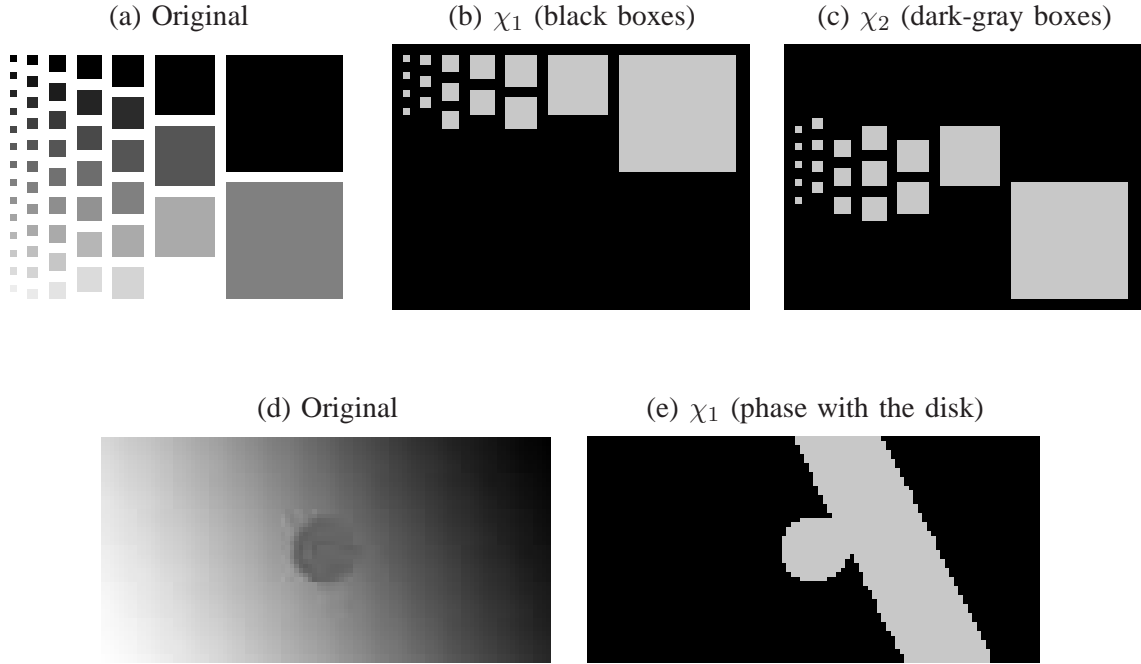


Fig. 2. The effect of \mathcal{S}_i : In the top row, from the given original image (a), two biggest boxes on the right (one black and another gray) are identified as two different phases χ_1 and χ_2 . Then, all the black boxes will be in phase χ_1 (image (b)) and the similar intensity gray boxes are in phase χ_2 (image (c)). (These two phases χ_1 and χ_2 are two among many other phases, full results showing all other phases are in Figure 4.) In the second row, from the original image (d), one disk in the center is identified as one phase, together with all the similar intensity area. (The result showing all other phases are in Figure 3.)

To meet our objective of identifying significant size objects while minimizing a functional, we use the *inverse scale term*,

$$\mathcal{S}_i := \frac{P(\chi_i)}{|\chi_i|}, \quad (3)$$

where $P(\chi_i)$ denotes the perimeter of a phase χ_i and $|\chi_i|$ denotes the 2-dimensional area of a phase χ_i . By minimizing this term, the segmentation prefers to identify bigger objects rather than the smaller ones. For example, in Figure 2 (a), the biggest objects are the two big boxes (one black and another gray) on the right. Therefore, segmentation would identify the black box to be in one phase (for example, χ_1) and the gray box in another phase, χ_2 . Then, since the segmentation is driven by the intensity value, the similar intensity boxes will go the corresponding phase: black boxes into phase χ_1 and dark gray boxes into phase χ_2 . Also, in Figure 2 (d), the given image has only one definite object, the disk in the center, so this object and similar intensity areas are identified as one phase χ_1 .

Remark 1: The inverse scale \mathcal{S}_i is defined on each phase χ_i , thus it is possible to have disconnected regions within the phase. We compute the total length of the edges in the phase χ_i and divide by the total area of objects in the phase χ_i , regardless of how many connected component this phase χ_i has. For example, several different objects with similar intensities will be in one phase χ_i and contribute to \mathcal{S}_i all together.

Remark 2: This notation of \mathcal{S}_i is related to the *Cheeger Set*, which is widely studied in calculus of variation analysis. The objective is to find a nonempty set $A \subset \Omega$ of finite perimeter which minimizes the following,

$$\min_{A \subset \Omega} \frac{P(A)}{|A|}.$$

There are various studies on qualitative properties of Cheeger Sets, and [4], [8] give good overviews and some references for related recent works on Cheeger sets. By defining a finite perimeter $\lambda := \frac{P(G)}{|G|}$, and considering $\min_{A \subset \Omega} P(A) - \lambda|A|$, these studies of Cheeger sets are related to Total Variation minimization, $\min_{u \in BV(\Omega)} \int_{\Omega} |Du| + \lambda \int_{\Omega} |u(x) - u_o(x)|^2$, which is consistent with the scale notation studied in [25]. Note, these Cheeger Set studies are only on one set A , while our interests are in multiple sets of these kinds.

Property 1: For a phase χ_i with a single object, if the perimeter is fixed, convex object have smaller \mathcal{S}_i compared to the concave objects. Therefore, by minimizing \mathcal{S}_i the shape of object prefers to be closer to a circle rather than an ellipse.

Property 2: Objects with different shape can have the same inverse scale value. For example, any regular (equilateral) convex polygon, B , which incircles a circle with radius r has $\frac{P(B)}{|B|} = \frac{2}{r}$, which is the same as the inverse scale value of a circle with radius r .

B. Balance

In order to give balance among the phases, we do not assume any particular importance among different phases, and we consider the summation without any particular weight,

$$\sum_{i=1}^K \mathcal{S}_i = \sum_{i=1}^K \frac{P(\chi_i)}{|\chi_i|}.$$

Then, for a given discrete bounded image with $|\Omega| < \infty$ and $\sum_{i=1}^K P(\chi_i) < \infty$, for a fixed K , the minimum of the summation is achieved when \mathcal{S}_i are all equal to each other for $\forall i = 1, \dots, K$. Therefore, by minimizing this term, the objects of various sizes in the image will uniformly be distributed among all

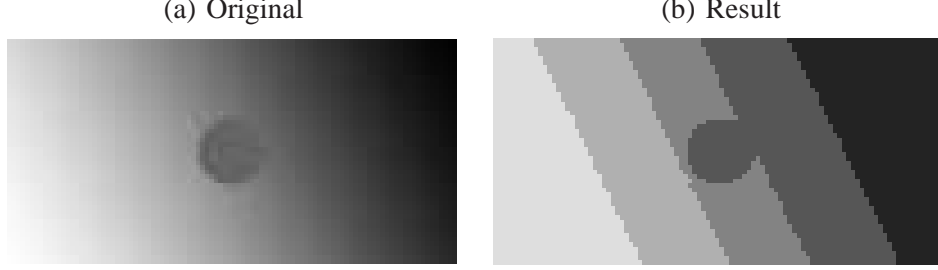


Fig. 3. The effect of $\sum \mathcal{S}_i$: The original image (a) has a smooth background with a disk in the center. (b) is the segmented result $\sum c_i * \chi_i$, using the proposed model (5). A phase with the disk is identified, as in Figure 2 (e), and the remaining background is more or less uniformly divided as shown in image (b).

different phases and \mathcal{S}_i value will be similar to each other. We refer to this term as *the phase balancing* term, since it prefers to find balance among the scales of each phases. Figure 3 shows this effect of uniform separations among the phases.

Proposition 1: For a fixed K , given a piecewise constant image with multiple objects B_j with the same ratio, $P(B_j)/|B_j| := p_1$ (except for the background), any distribution of these objects B_j to different phases χ_i (no empty phases, no partial objects) gives minimum of the phase balancing term, and

$$\sum_{i=1}^K \frac{P(\chi_i)}{|\chi_i|} = (K-1)p_1 + \frac{P(\chi_b)}{|\chi_b|},$$

where χ_p represents the background.

Proof: The inverse scale term \mathcal{S}_i in (3) is define for each phase, not for each object. For example, if one phase χ_i has one circle with radius r , $\mathcal{S}_i = 2/r$, and if another phase χ_j has two circles, $\mathcal{S}_j = \frac{2\pi r + 2\pi r}{\pi r^2 + \pi r^2} = 2/r$. Therefore, if we let the length of an object to be $P(B_j) = a$, the area to be a/p_1 and m_i be the number of the objects in the phase χ_i , then, $\mathcal{S}_i = m_i a / m_i (a/p_1) = p_1$, independent of the number m_i . The phase balancing term will be $(K-1)p_1$ except for the phase representing the background. ■

According to above Proposition, if an image has only one kind of object, the number of objects in each phases can be quite different, which can be counter-intuitive to the balancing effect. This is due to the way we compute the \mathcal{S}_i (Remark 1).

C. The proposed model

Incorporating these additional objectives, we propose the following functional for automatic multiphase segmentation, *a phase balancing model*,

$$E[K, \chi_i, c_i | u_o] = \hat{\mu} \left(\sum_{i=1}^K \mathcal{S}_i \right) \mathcal{H}^1(\Gamma) + \sum_{i=1}^K \int_{\chi_i} |u_o - c_i|^2, \quad (4)$$

where Γ is set of all the boundaries of χ_i for $i = 1, \dots, K$, i.e. $\Gamma = \bigcup_{i=1}^K \{\partial\chi_i\}$, \mathcal{H}^1 represents the 1-dimensional Hausdorff measure as in (1) and (2), and the average value c_i s are defined as in (2), $c_i = \int_{\chi_i} u_o(x) dx / \int_{\chi_i} 1 dx$. Notice that K , χ_i s and c_i s in $E[K, \chi_i, c_i | u_o]$ are unknown variables while only the original image u_o is given. This is one of the main difference compared to the other multiphase models, which don't minimize the functional with respect to the number of phases K . Using $P(A)$ to represent the finite perimeter of the set A , the proposed functional can be also represented as

$$E[K, \chi, c_i | u_o] = \mu \left(\sum_{i=1}^K \frac{P(\chi_i)}{|\chi_i|} \right) \sum_{i=1}^K P(\chi_i) + \sum_{i=1}^K |u_o - c_i|^2 \chi_i. \quad (5)$$

Here $\mu = \hat{\mu}/2$ from $\hat{\mu}$ in (4), since by adding the perimeter of each phases the length of boundaries will be added twice.

In this functional, μ is the only free parameter, and for an unsupervised segmentation we typically set $\mu = 1$. The first term of (5) is essentially unit-free, while the second term $\sum_{i=1}^K |u_o - c_i|^2 \chi_i$ corresponds to the area of the phase, therefore, this μ is a parameter representing the area of the segmentation. If μ is big, the segmentation prefers to have phases with bigger areas, and smaller value for μ prefers smaller phases for a segmentation. The effects of this changes of μ are explored in Section IV, and for unsupervised segmentation we kept this $\mu = 1$.

To illustrate the full effect of this model, we consider the example in Figure 2 again. After the two main features are identified, the other regions are well divided to give balance among the phases and follow the intensity differences. Figure 4 illustrates the full result. The original image Figure 2 (a), has at least 15 different intensity values, however, the image is automatically (with $\mu = 1$) identified to 4 different phases. The segmentation is driven by the two biggest objects, then the rest are well distributed following the intensity similarities while giving the balance among the phases.

Remark 3: In the proposed model (5), the perimeter $P(\chi_i)$ appears twice, once in the phase balancing term and the total length term. According to the Property 2 in subsection II-A, the smoothness of the boundary is independent to minimizing \mathcal{S}_i , since the circle and a convex polygon can have the same

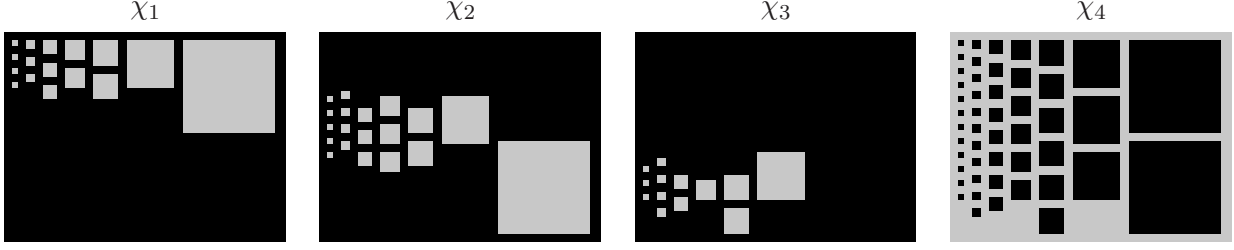


Fig. 4. In the original image Figure 2 (a), each column of boxes are changing the intensity consistently from top to bottom, and the size of the boxes are increasing from left to right (length of the width is doubling each time). These images are identified phases using the proposed model. The model automatically chooses four phases with $\mu = 1$, and it shows that the boxes are well distributed among the phases. Notice the strong similarity among the phases.

inverse scale value. Therefore, the total length term $\mathcal{H}^1(\Gamma)$ is needed for its smoothness property (and well-fitted boundaries).

Remark 4: As shown in Figure 3 and 4, the segmentation is mainly driven by the intensity. The model favors larger continuous region, however, the smaller regions with similar intensity will also go into the same phase. The small objects, such as noise or small stars, have a big inverse scale value, and it will be identified as a feature of the image rather than being completely denoised. Denoising occurs within a certain difference in intensity. If the intensity is close to one of the phases, it will be included in that phase. (See Figure 12).

Remark 5: After proposing to add two additional objectives in the form of the phase balancing term, $\sum_{i=1}^K \mathcal{S}_i$, we had different options to modify the new functional. For example, Case I, adding (not multiplying) the phase balancing term to CV model (2): this loses the unsupervised properties and the results become heavily depended on the choice of two parameters, β and μ . This inherits limitations of CV model with additional parameter to choose. Case II, multiplying $\sum \frac{1}{\mathcal{S}_i}$ to the total length term, i.e. two terms in the segmentation function both represents the area, and Case III, multiplying the phase term to the fitting term, i.e. both terms represents length of the segmentation. In these both cases, Case II and Case III, in addition to being sensitive to the choice of the parameter, we observed that the number of phase K increases to minimize to energy. The total length term is never zero, while the fitting term can become zero by increasing the number of phases continuously, therefore, both cases typically result in a big number of phases.

In the following section, we present a brute-force algorithm for a fast and easy computation of the

proposed model (5).

III. FAST ALGORITHM FOR MULTIPHASE SEGMENTATION

As before, each phase is a separate characteristic function χ_i , for $i = 1, \dots, K$, and represent the segmented result as $u = \sum_{i=1}^K c_i * \chi_i$. Typically, a level set method is widely used in these settings [7], [16], [19], [20], [26], [28], or one function is used to represent multiphases as in [13], [16]. However, by using each characteristic function χ_i to represent each phase, this allows simplicity in adding new phases and does not introduce bias in transition from one phase to another.

This unsupervised segmentation model (5) is nonlinear and non trivial to identify the Euler-Lagrange equation with three different types of unknowns: the number of phases K , χ_i s and the average intensity c_i s. Thus, we decided to accentuate the speed and simplicity by directly minimizing this functional. We are not the first to use these fast techniques, and the credit goes to [11], [24], which discuss applications to level set implementation in two phase identification. In particular, we adapted the main idea of Song and Chan [24] to consider the change in the difference of the functional using a greedy algorithm to decide if one pixel belongs to the inside or the outside of the contour. These settings, [11], [24], are well-equipped to handle fast computation for two phase computations. In [12], the authors used fast algorithm for multiphase level set method for CV model, and discuss the danger of using these algorithms for the length term via considering the topological derivative. (In this paper, we extend the idea of [24] to multiphase model, and work with the discrete setting of the functional that the length change is explicitly computed by the four edge changes.)

From the proposed model (5),

$$E[K, \chi, c_i | u_0] = \mu \left(\sum_{i=1}^K \frac{P(\chi_i)}{|\chi_i|} \right) \sum_{i=1}^K P(\chi_i) + \sum_{i=1}^K |u_0 - c_i|^2 \chi_i,$$

we consider the difference in the functional and pick the phase according to the minimum value. For $(x, y) \in \Omega$, the change in energy when (x, y) moves from one phase l to another phase j is computed by,

$$\Delta E_{lj} = \mu \Delta ST + (u - c_j)^2 \frac{n_j}{n_j + 1} - (u - c_l)^2 \frac{n_l}{n_l - 1}, \quad (6)$$

where $u = u(x, y)$ is the intensity value at the pixel (x, y) , c_i is the average of each phase i , and n_i is the number of pixels in phase i , i.e. area $|\chi_i| = n_i$. The first term ΔST is the change of the phase balancing and total length term in (5), and other two terms are the change of the intensity fitting term which is used in [24].

Then, this ΔST is

$$\Delta ST = S_j T_j - S_l T_l = S_j(T_l + \Delta T) - S_l T_l = (S_j - S_l)T_l + S_j \Delta T = T_l \Delta S + S_j \Delta T,$$

where S_l presents the phase balancing energy ($\sum S_i$) and T_l the total length energy ($\sum P(\chi_i)$) when (x, y) is in phase l . To compute the total length T_l , since each phase is represented by a characteristic function χ_i , we simply add all the edges in the phase to get the length,

$$P(\chi_i) = \sum_{(x,y) \in \Omega} \{|\chi_i(x+1, y) - \chi_i(x, y)| + |\chi_i(x, y+1) - \chi_i(x, y)|\}$$

then, when the pixel is in phase l , $T_l = \sum_{i=1}^K P(\chi_i)$ and $S_l = \sum \frac{P(\chi_i)}{n_i}$.

The difference in total length energy, ΔT becomes an addition of the change of perimeter in phase j and the change in phase l , $\Delta T = \Delta P(\chi_j) + \Delta P(\chi_l)$. In phase j , if pixel (x, y) changes from 0 to 1, the change in the length can be computed from the values of the neighboring points, i.e. $\Delta P(\chi_j) = 4 - 2 \sum_{(a,b) \in \mathcal{N}} \chi_j(a, b)$, where \mathcal{N} refers to four neighboring points (N,S,E,W of (x,y)). When there were no edges ($\forall (a, b) \in \mathcal{N}, \chi_j(a, b) = 0$), by changing this pixel from 0 to 1, it creates four new edges. If there is one edge, by flipping $\chi_j(x, y) = 0 \rightarrow 1$, it creates two additional edges. If there were two edges, the change creates no new edges, but if there were four edges, it will remove those four edges (-4). Similarly, change in the perimeter of phase l becomes $\Delta P(\chi_l) = -4 + 2 \sum_{(i,j) \in \mathcal{N}} \chi_l(i, j)$. Then, the difference in the total length becomes

$$\Delta T = -2 \left(\sum_{(i,j) \in \mathcal{N}} \chi_j(i, j) - \sum_{(i,j) \in \mathcal{N}} \chi_l(i, j) \right). \quad (7)$$

The difference ΔE_{lj} in (6) can be computed by gathering all these terms,

$$\Delta E_{lj} = \mu(T_l \Delta S + S_j \Delta T) + (u - c_j)^2 \frac{n_j}{n_j + 1} - (u - c_l)^2 \frac{n_l}{n_l - 1}. \quad (8)$$

This is an explicit difference of the energy when the pixel changes from one phase l to another phase j , which is used in the algorithm, Table I (9). If $\Delta E_{lj} > 0$, the pixel will not change to phase j since that will increase the energy. While, if this value ΔE_{lj} is negative, it is better to move (x, y) to phase j .

In this algorithm, we are considering multiphase segmentation, it is important to noticed that the number of phases are initially set to be $K = 1$ for all the experiments. In Table I, the algorithm compares the change ΔE_{lj} among all the existing different phases $j = 1, \dots, k$ and if necessary, it creates a new phase to minimize the energy. This new phase is represented as phase $k + 1$ and the difference in the energy (9) is calculated using $n_{k+1} = 0$.

Algorithm

- Set an initial phase: $|\chi_1| = |\Omega|$ with $k_o = 1$, where k_o is the number of phase.
- Iterate
 - 1) At each pixel $(x, y) \in \Omega$ which belongs to phase l ($\chi_l(x, y) = 1$ and $\chi_i(x, y) = 0$ for $\forall i \neq l$), compute

$$value = \min_j \{\Delta E_{lj} | j \neq l, j = 1, \dots, k+1\}, \quad (9)$$

and let $h = \text{arg min}_j \{\Delta E_{lj} | j \neq l, j = 1, \dots, k+1\}$. Here $k+1$ refers to the new empty phase.

Then,

$$\begin{cases} \text{if } value < 0, & \text{set } \chi_h(x, y) = 1 \text{ and } \chi_l(x, y) = 0. \\ \text{if } value > 0, & \text{do nothing} \end{cases}$$

- 2) Update $k = h$, calculate $n_i = |\chi_i|$ and c_i for each phase $i = 1, \dots, k$.

TABLE I

A PIXELWISE BRUTE-FORCE ALGORITHM

The complexity of the algorithm is straightforward. Let m be the total number of pixels in the image. At the first pixel, it was two choices: the current phase χ_1 and a new phase χ_2 . As the algorithm sweeps through the domain, at each pixel it was $k+1$ choice of phases, where k is the current number of phases and one additional choice for a new phase. For the most brute-force algorithm, when the number of phases is fixed as r , the complexity is $\mathcal{O}(rm)$, and when the number of phases is increasing with each iteration, the complexity becomes $\mathcal{O}(m + 2m + \dots + sm)$ where s is the maximum number of regions attempted. The second type of method ends up being $\mathcal{O}(s^2m)$. However, for the proposed algorithm, the number of phases is typically identified after only one sweeping of the image, the complexity calculation is $\mathcal{O}(km) = \mathcal{O}(m)$ for upto k number of phases. This is also similar to the fast algorithm method [24] which gives $\mathcal{O}(m)$ complexity.

The proposed method allows for a real-time processing of a large image set, since there is no need to pre-process the data to identify the number of regions, but it is automatically given from the iteration. The run time on a single core Intel processor computer for 100 by 100 image is 100 frames/second using C++. Typically, the algorithm converges in less than 6 iterations.

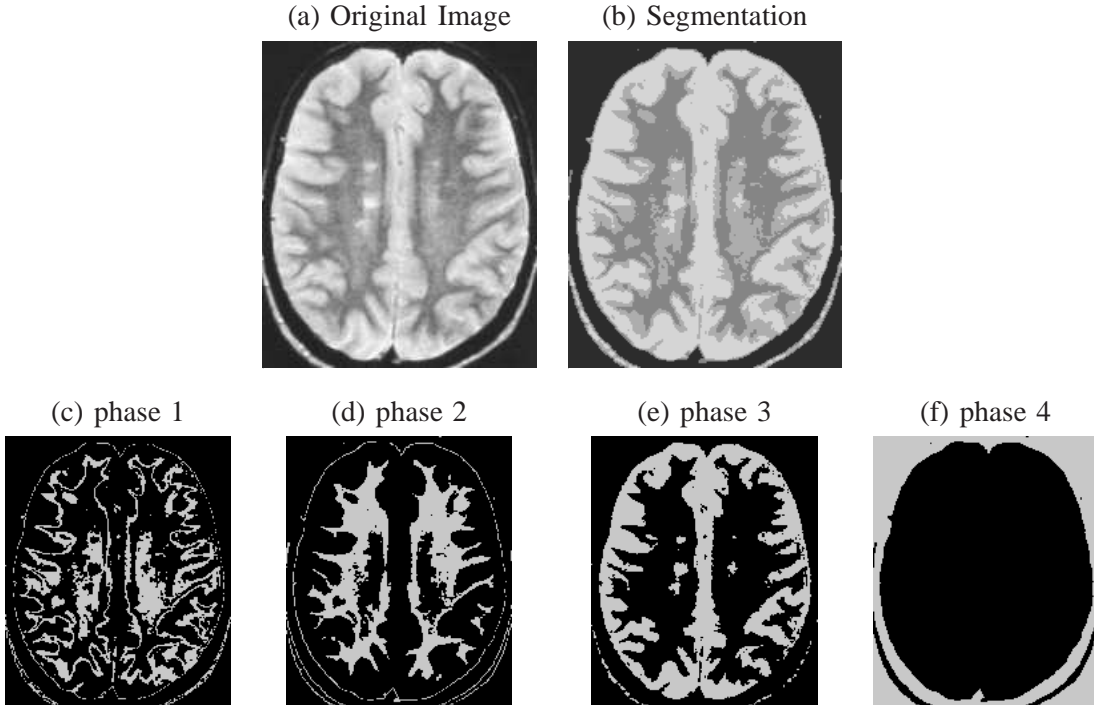


Fig. 5. Real image: A MRI brain image is automatically segmented into four regions. The model segments the different parts of the brain accurately.

IV. NUMERICAL EXPERIMENTS

All of the experiments are initialized with $|\chi_1| = |\Omega|$ i.e. $K = 1$, and most of the experiments were done with $\mu = 1$ (unless otherwise stated). The following experiments are done with left to right, and down sweeping order. These conditions eliminate some of the difficulties associated with multiphase segmentation.

Figure 5 shows an experiment on a real image, a MRI brain scan. The model not only automatically gives four phases, but also segments the different parts of the brain accurately. Figure 6 shows that the model segments the image with sharp corners and clear edges. This model automatically identifies five phases: white, gray, black (blue), green and yellow.

This method is extended to color images in Figure 6. As in [5], we added all the channels for this experiment, using

$$\mu \left(\sum_{i=1}^K \frac{|\partial\chi_i|}{|\chi_i|} \right) \sum_{i=1}^K |\partial\chi_i| + \sum_{i=1}^K \int_{\chi_i} \sum_{l=1}^3 |u_{0,l} - c_{i,l}|^2 dx, \quad (10)$$

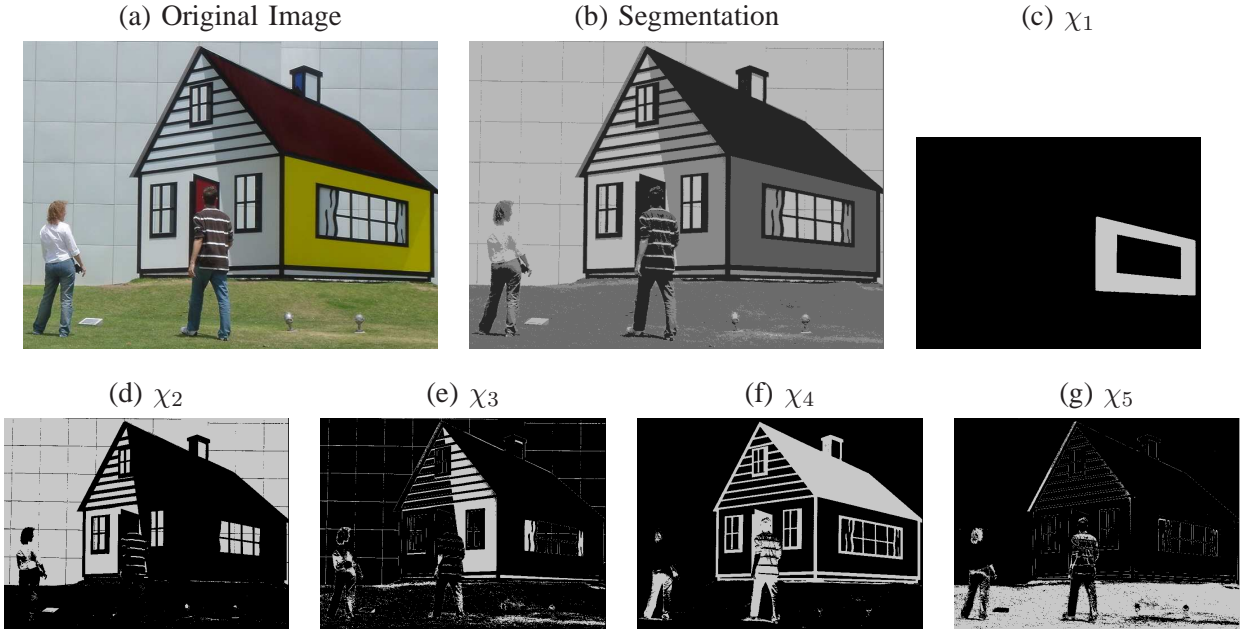


Fig. 6. Color image: The model automatically segments the original image to five phases. Each segments refers to χ_1 (yellow), χ_2 (white), χ_3 (gray), χ_4 (black/blue) and χ_5 (green). The model is extended to a vector model using the fitting term as in [5], and for the image with sharp corners and edges, this model successfully finds shape boundary information.

here index l refers to each RGB (red, green and blue) channels.

The proposed model automatically picks an appropriate number of phases depending on the image. In Figure 7, the original image (a) is automatically segmented to 4 phases (blue, white, yellow and green). And when zoom into the one phase the field region (yellow), image (c), is automatically further segmented to three phases. This shows that the proposed model (5) adjusts to the given image and recognizes or not recognizes certain features depending on the focus.

A. Application to image quantization

The proposed model can be applied to image quantization. Image quantization is used when high-resolution images are displayed on low-resolution or low-bit devices, such as in the calculators or in cell phones. If the low-bit device is a q -bit device, the range of the image can only take few discrete values from 0 to $2^q - 1$. With vast developments in cell phones and hand-held devices, good quality and fast quantization became more important. Figure 8 shows such an application. Using this model, the image is automatically segmented to five phases. In [22], the authors computed the segments by minimizing the

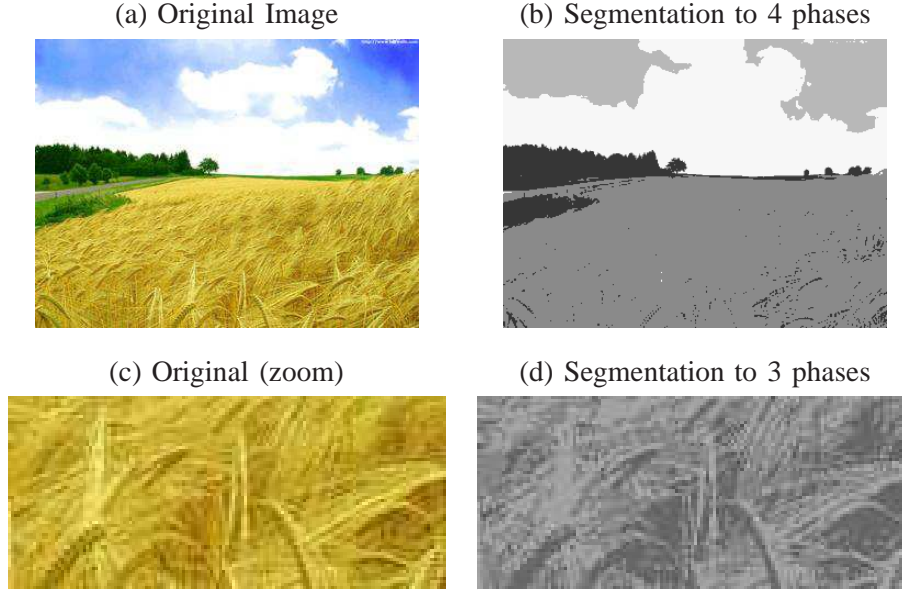


Fig. 7. Focus of the image: The original image (a) is automatically segmented to 4 phases in image (b). When zoom into the one phase the field region (yellow), image (c), is automatically further segmented to three phases in image (d). The model adjusts to the given image and recognizes or not recognizes certain features depending on the focus.

TV functional which is constrained on the quantum set Q . Here the cardinality K is given.

$$\min_{u \in BV^Q} E[u] = \min_{u \in BV^Q} \int_{\Omega} |Du| + \frac{\lambda}{2} \int_{\Omega} (f - u)^2 dx,$$

where $BV^Q = BV(\Omega; Q) = \{u \in BV(\Omega) : u(x) \in Q, \text{ a.e. } x \in \Omega\}$. With the given cardinality $K = 6$, the girl image is quantized with method [22] (Figure 8, image (c)) and the optimized quanta set is found to be $Q = \{0.1314, 0.2860, 0.4514, 0.6009, 0.7484, 0.9417\}$. In our experiment, Figure 8, image (a) is automatically segmented to six phases in image (b), and the c_i values are found to be $\{0.1468, 0.2915, 0.4628, 0.6121, 0.7554, 0.9508\}$ these values are within 2% difference. This example shows an application of the unsupervised segmentation model to image quantization.

B. The number of phase K : automatic stopping

Notice from the algorithm, Table I, that initial condition is always set as $K = 1$ with $\chi_1 = \chi_{\Omega}$, and as the algorithm sweeps through the domain the number of phases increases. It is important to understand when the algorithm stops adding the new phase, to automatically give a reasonable number of phases K .

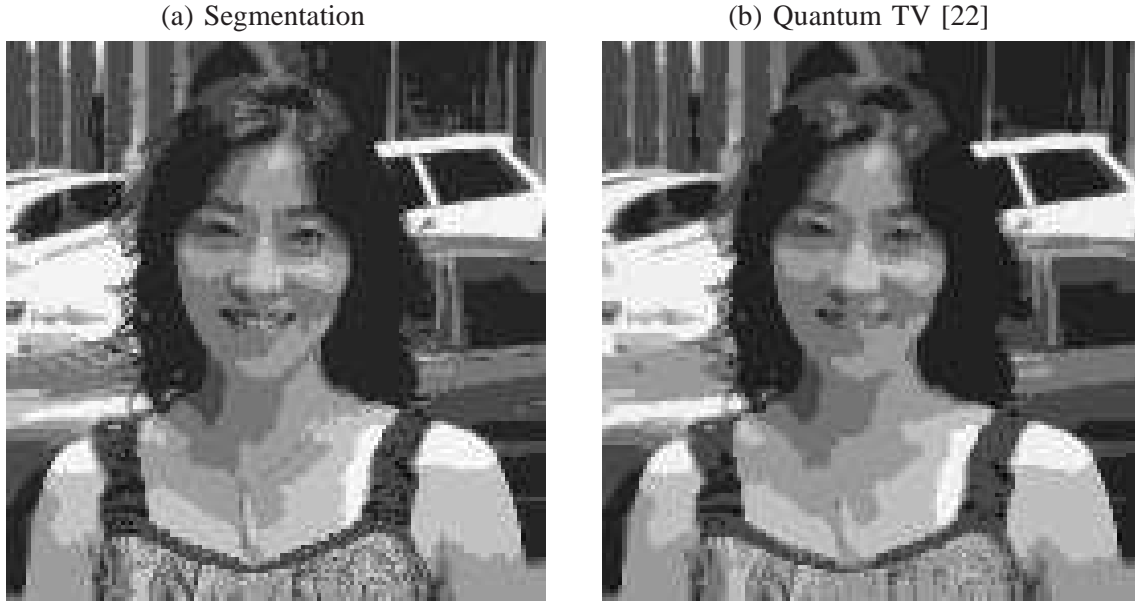


Fig. 8. Image quantization: The proposed model can be applied to image quantization. This model automatically segments the image to six phases. Compared to Quantum TV [22], this model keeps more details and features of the original image, such as the necklaces, details of the face and texture of the clothing.

In the algorithm (9), a new phase is created only if it gives the minimum of ΔE_{lj} among all possible choices of i, j , and also if that minimum is a negative value. Therefore, we look into the details of when the energy becomes negative for possibly creating a new phase, i.e. $\Delta E_{lj} < 0$, for $j = k + 1$ and $n_j = 0$. For this new phase, the intensity difference is zero, $(u - c_j)^2 = 0$, and the energy (8) is negative when

$$\mu(T_l \Delta S + S_j \Delta T) \left(1 - \frac{1}{n_l}\right) < (u - c_l)^2, \quad (11)$$

for at least one $l \leq k$. This left-hand-side value, $test := \mu(\Delta ST) \left(1 - \frac{1}{n_l}\right)$ gives the lower bound on how big the intensity difference (between the current pixel $u(x, y)$ and each phase intensity average c_l) should be to create a new phase $j = k + 1$. First of all, as n_l increases (as the area of existing phase gets bigger), the $test$ increases, so it requires the intensity to be more different from averages c_l to create a new phase by itself. Secondly, the $test$ value is depended on ΔS multiplied by T_l , so, when the segmentation is already complicated with a large total length T_l , it becomes more difficult to add a new phase. Thirdly, ΔT is multiplied by S_j , and since the new phase j only have one pixel, this S_j is quite big. After this test (11) is satisfied, the energy ΔE_{lj} still needs to be the minimum among all other possibilities of

being added to different phases.

To summarize, as the size of the phases increases, it becomes more difficult to add new phase. As soon as all the phases reach certain sizes, the algorithm's sensitivity to the intensity fitting term decreases, and prefer to be added to already existing phases. This is independent to the location of the regions, since the area and perimeter is computed over each phase without considering the local connected components separately. This is the main reason for the automatic selection of K and the proposed functional gives unsupervised segmentation.

As a comparison, we considered the reduced piecewise constant Mumford-Shah, Chan-Vese [6] model as in [7]. We designed a similar brute-force algorithm as (8) for multiphase CV model,

$$\Delta\mathcal{E}_{cv} = \beta\Delta T + (u - c_j)^2 \frac{n_j}{n_j + 1} - (u - c_l)^2 \frac{n_l}{n_l - 1} \quad (12)$$

and we find that this algorithm also works very well if the original image is a piecewise constant function. However, for non-piecewise constant images, these type of brute-force algorithm seems to continuously add new phases, or the algorithm becomes very sensitive to the choice of parameter β . This can be seen from a similar analysis as (11). The energy is negative, when

$$\beta \Delta T \left(1 - \frac{1}{n_l}\right) < (u - c_l)^2.$$

It is clear this algorithm will be sensitive to the choice of β . Since this test is only depended on the change in total length, which is typically very small, unless big β is given, this algorithm will continue to add new phases. In (2), this effect corresponds to the intensity fitting term going to zero as more and more phases are added. Therefore, big enough β should be given, and the result will be very sensitive to this choice.

Figure 9 illustrates this comparison. Given a image (a), the proposed model segments the image with 5 phases automatically, while as in image (c), the CV model using a brute-force algorithm (12) will continue to increase the number of phases. Even with a big value of β which resulted in quite a denoised result, this image (c) has about 128 number of phases with many small regions. However, when the phase number is given for CV model, in this case $K = 5$, the brute-force algorithm (12) becomes less sensitive to the choice of β and gives a good segmentation result. Comparing image (b) and image (d), our proposed model gives comparable result to CV model, with unsupervised K .

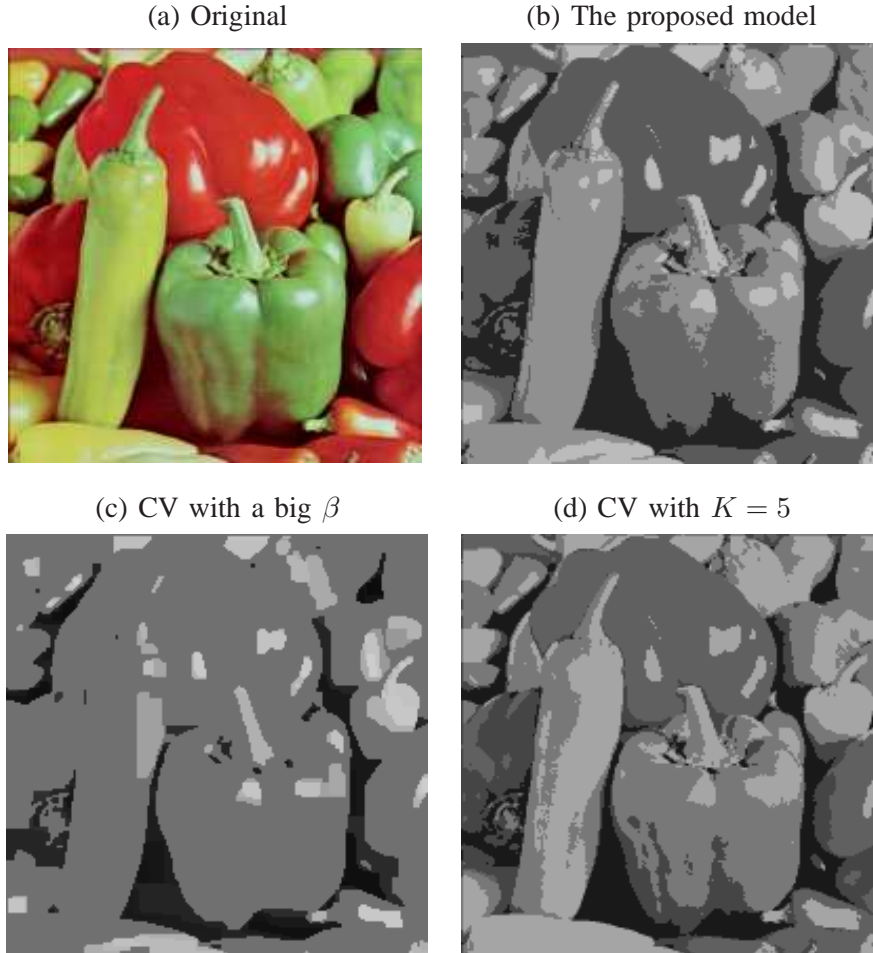


Fig. 9. Comparison: (a) The original image. (b) Using (6), the proposed unsupervised model. (c) Using CV model with a brute-force algorithm (12) using a big β (d) Using CV model with (12) for a given fixed number of phase $K = 5$. Comparing image (b) and image (d), the proposed model gives comparable result to CV model. With the number of phases K is not given for CV model, in image (c) the methods continuous to add new phases even with a big number of β . This image (c) has about 128 phases, many of which are very small regions.

C. The effects of different μ

Up to now, all the experiments were using $\mu = 1$. This makes the proposed model (5) essentially parameter free. By changing μ , different results can be achieved as in Figure 10. Compared to the Figure 7 (b) $\mu = 1$, Figure 10 (b) using $\mu = 10$ returns only two phases separating the sky from the earth. On the other hand, by decreasing the μ to 0.1 in Figure 10 (c), the proposed model gives more detailed separations and identifies ten different phases.

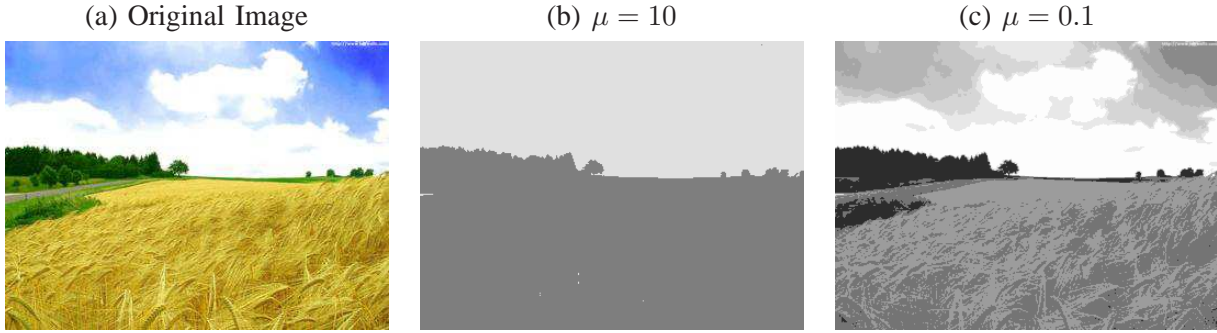


Fig. 10. Different μ : Bigger values of μ give bigger regions for segmentation. When $\mu = 10$, the model gives only two phases separating the sky from the earth (white and blue, and yellow and green regions are merged). While by using $\mu = 0.1$, the model enforces the intensity fitting term, and it gives ten phases with more detailed separations of the image.

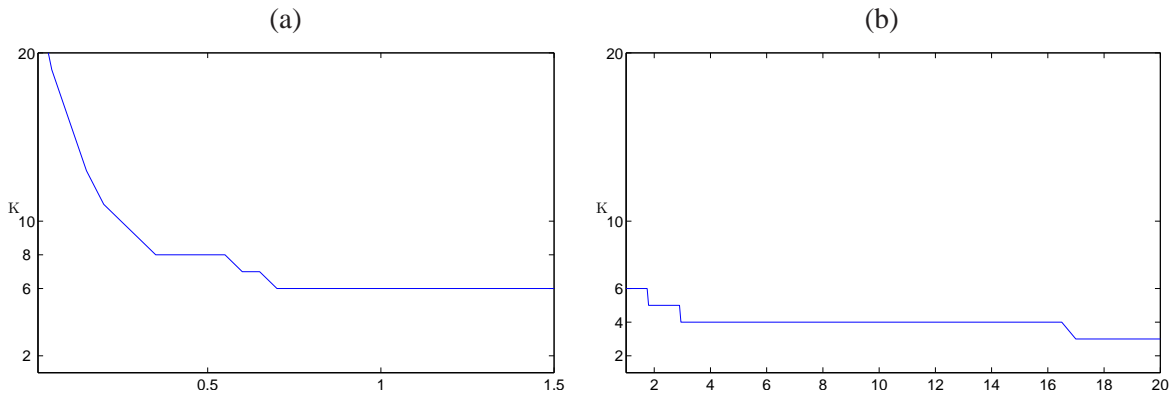


Fig. 11. K verses μ : The plots of K verses μ for the girl image in Figure 8. The range of μ are (a) $0.01 < \mu < 1.5$ and (b) $1 < \mu < 20$. Notice that each piecewise intervals are quite large showing this model is not very sensitive to the choice of μ .

Since we are varying the parameter μ , we present a plot in Figure 11 to show the changes in the phase number K verses different μ values. We experimented with the girl image in Figure 8. Both graphs are a plot of the number of phases K verses the μ values, (a) $0.01 < \mu < 1.5$ and (b) $1 < \mu < 20$. As predicted in Figure 10 (also related to the inequality (11)), this is a decreasing function, and to have an integer value K , the graph becomes a step function. Notice, that each piecewise intervals are quite large showing this model is not sensitive to a careful choice of μ .

Using different values of μ , the proposed model can also handle a cluster segmentation. Figure 12 shows an example of segmentation of a nebula (this is a color image and vector-valued model (10) is

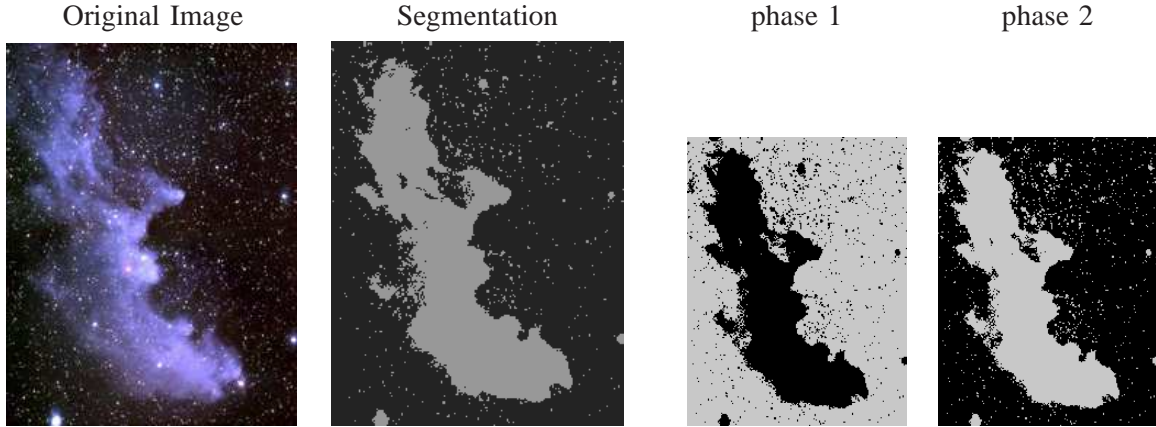


Fig. 12. Cluster segmentation: A color image of a nebula is segmented into two phases using $\mu = 10$. Notice the details of the boundaries are kept while other small stars within the cluster is denoised and identified as the part of the main cluster.

used.). Using $\mu = 10$, the image is segmented into two regions (while using $\mu = 1$, it gave 6 different phases). Notice the details of small stars are kept as a part of identified nebula. This is due to the way we compute the phase length and area (not considering each connected components separately), and as mentioned in Section II-C, Remark 4 only the small objects which has similar intensities as the identified phase will be kept, while others are denoised. Noticed the bright starts within the nebula is included in the phase without being identified separately, showing this model have denoising effect while keeping details of the boundary.

D. Histogram comparison

Without an unsupervised model, one way to give a phase number a priory is to consider the image's histogram. Therefore, we compare the histogram of original image and the histogram of the segmented image to see the effect of the proposed model. In Figure 13, the blue dotted line is the histogram of the original image and the red solid line is the histogram of the segmented result. For the images, such as he girl (b), it is not totally clear how many phases are needed just from the histogram, nevertheless, the proposed model picks a reasonable number of phases.

This example also shows the difference between the proposed model and the typical k-mean or GMM methods. The image segmentation and data mining are two different applications and the minimization functional and the objective is somewhat different. However, the similarities lies in the fact that there is a

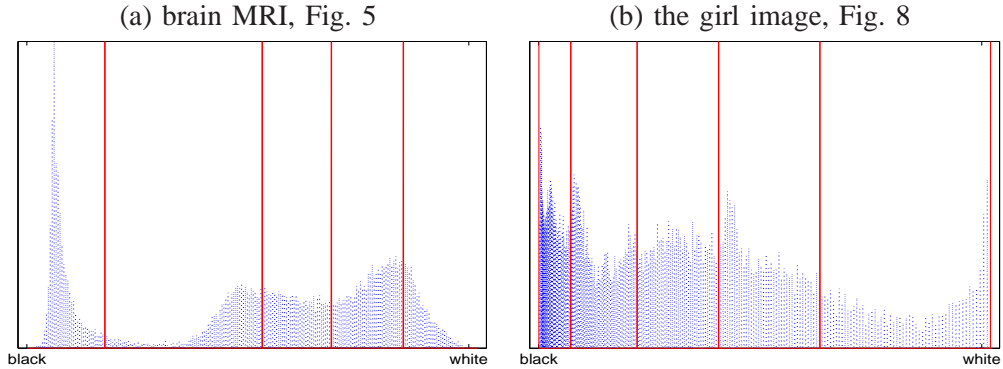


Fig. 13. Histogram comparison: The blue dotted lines are the histogram of the original image, and the red solid red lines are the histogram of the segmented result (i.e. c_i values). The range of the y-axis is artificially shortened to show the details, i.e. the red lines have a bigger value than represented in these graphs. Looking at the histogram of the original images, it is might be unclear how many number of phases are needed for the segmentation. Image (a) and (b) show that the proposed model automatically gives reasonable number of phases as well as the locations of c_i .

number of bins (or phases) to choose (this connection is also mentioned in [11]). Most of these methods, the number K is given a priori, then after iterations they correct the locations, or many pre-processing and learning process is added before these methods are used. However, in the proposed model, the number of phases K is given from the minimization of the proposed functional. This proposed functional has a fitting term and a regularization term with newly added phase balancing term, which allows the automatic segmentation.

V. CONCLUSION

We propose a new unsupervised multiphase segmentation model that balances each phases and automatically gives a reasonable number of phases. One limitation of many multiphase segmentation methods is in choosing the number of phases needed for the segmentation.

By adding two additional objectives, we achieved automatic segmentation which gives a reasonable number of phases K and finds each phase. This proposed method have interesting properties and many different extensions and applications are possible. To find the minimum of this nonlinear functional, we used a brute-force algorithm for a fast and accurate computation. The algorithm gives an insight on why this model has automatic stopping criteria for choosing the number of phases K . We experimented with syntactic and real images, considered applications to image quantization, extension to color images, and

cluster segmentation.

This work marks a beginning of research in this area. By identifying the number of phases for a segmentation, many new and interesting applications are possible. This includes combining k-means with this clustering method for data mining applications and incorporating logic frameworks [19] in identifying key objects in the image. This furthers the pursuit of a robust and flexible computer vision system.

REFERENCES

- [1] E. Bae and X.-C. Tai. Graph cuts for the multiphase mumford-shah model using piecewise constant level set methods. *UCLA CAM Report 08-36*, 2008.
- [2] T. Brox and J. Weickert. Level set based image segmentation with multiple regions. In *Pattern Recognition*, volume 3175 of *Lecture Notes in Computer Science*, pages 415–423. Springer Berlin / Heidelberg, 2004.
- [3] T. Brox and J. Weickert. A TV flow based local scale measure for texture discrimination. In *Computer Vision - ECCV 2004*, volume 3022 of *Lecture Notes in Computer Science*, pages 578–590. Springer Berlin / Heidelberg, 2004.
- [4] V. Caselles, A. Chambolle, and M. Navaga. Uniqueness of the cheeger set of a convex body. *Pacific Journal of Mathematics*, 232(1):77–90, 2007.
- [5] T. Chan, B. Sandberg, and L. Vese. Active contours without edges for vector-valued images. *Journal of Visual Communication and Image Representation*, 11:130–141, 1999.
- [6] T. Chan and L. Vese. Active contours without edges. *IEEE Transactions on Image Processing*, 16(2):266–277, 2000.
- [7] J. Chung and L. Vese. Image segmentatin using a multilayer level-set approach. *UCLA CAM Report 03-53*, 2001.
- [8] A. Figalli, F. Maggi, and A. Pratelli. A note on cheeger sets. *Proc. Amer. Math. Soc.*, 137:2057–2062, 2009.
- [9] S. Gao and T.D. Bui. Image segmentation and selective smoothing by using Mumford-Shah model. *IEEE Transactions on Image Processing*, 14(10):1537–1549, 2005.
- [10] S. Geman and D. Geman. Stochastic relaxation, Gibbs distributions, and the Bayesian restoration of images. *IEEE Transactions on Pattern Analysis and Machine Intelligence*, 6:721–741, 1984.
- [11] F. Gibou and R. Fedkiw. Fast hybrid k-means level set algorithm for segmentation. *proc. of the 4th Annual Hawaii Int. Conf. on Stat. and Math.*, 2002.
- [12] L. He and S. Osher. Solving the Chan-Vese model by a multiphase level set algorithm based on the topological derivative. *Scale Space and Variational Methods in Computer Vision*, 4485/2008:777–788, 2007.
- [13] Y. M. Jung, S. H. Kang, and J. Shen. Multiphase image segmentation via Modica-Mortola phase transition. *SIAM applied Mathematics*, 67:1213–1232, 2007.
- [14] H. Li and X.-C. Tai. Piecewise constant level set methods for multiphase motion. *International J. Numer. Anal. Modelling*, 4(2):291–305, 2007.
- [15] J. Lie, M. Lysaker, and X.-C. Tai. A binary level set model and some applications to Mumford-Shah image segmentation. *IEEE Transactions on Image Processing*, 15(5):1171–1181, 2006.
- [16] J. Lie, M. Lysaker, and X.-C. Tai. A variant of the level set method and applications to image segmentation. *AMS Mathematics of Computation*, 75:1155–1174, 2006.

- [17] D. Mumford and J. Shah. Optimal approximation by piecewise-smooth functions and associated variational problems. *Commun. Pure Appl. Math.*, 42:577–685, 1989.
- [18] Yongsheng Pan, J. Douglas Birdwell, and Seddik M. Djouadi. Bottom-up hierarchical image segmentation using region competition and the mumford-shah functional. In *ICPR '06: Proceedings of the 18th International Conference on Pattern Recognition*, pages 117–121, Washington, DC, USA, 2006. IEEE Computer Society.
- [19] B. Sandberg and T. Chan. Logic operators for active contours on multi-channel images. *Journal of Visual Communication and Image Representation*, 15:333–358, 2005.
- [20] B. Sandberg, T. Chan, and L. Vese. A level-set and gabor-based active contour algorithm for segmenting textured images. *UCLA CAM report 02-39*, 2002.
- [21] J. Shen. Piecewise $H^{-1} + H^0 + H^1$ images and the Mumford-Shah-Sobolev model for segmented image decomposition. *AMRX Appl. Math. Res. Express*, 4:143–167, 2005.
- [22] J. Shen and S. H. Kang. Quantum TV and applications in image processing. *Inverse Problems and Imaging*, 1(3):557–575, 2007.
- [23] J. Shi and J. Malik. Normalized cuts and image segmentation. *IEEE Transactions on Pattern Analysis and Machine Intelligence*, 22(8):888–905, 2000.
- [24] B. Song and T. Chan. A fast algorithm for level set based optimization. *UCLA CAM Report 02-68*, 2002.
- [25] D. Strong, J.-F. Aujol, and T. Chan. Scale recognition, regularization parameter selection, and Meyer’s G norm in total variation regularization. *SIAM Journal on Multiscale Modeling and Simulation*, 5(1):273–303, 2006.
- [26] X.-C. Tai and T. Chan. A survey on multiple level set methods with applications for identifying piecewise constant functions. *International J. Numer. Anal. Modelling*, 1(1):25–48, 2004.
- [27] Z. W. Tu and S.C. Zhu. Image segmentation by Data-Driven Markov Chain Monte Carlo. *IEEE Transactions on Pattern Analysis and Machine Intelligence*, 24(5):657–673, 2002.
- [28] L. Vese and T. Chan. A multiphase level set framework for image segmentation using the mumford and shah model. *International Journal of Computer Vision*, 50(3):271–293, 2002.
- [29] S.C. Zhu and A. Yuille. Region competition: Unifying snakes, region growing, and bayes/mdl for multi-band image segmentation. *IEEE Transactions on Pattern Analysis and Machine Intelligence*, 18:884–900, 1996.